COMPARING TWO NUMERICAL MODELS IN SIMULATING HYDRODYNAMICS AND SEDIMENT TRANSPORT AT A DUAL INLET SYSTEM, WEST-CENTRAL FLORIDA

PING WANG[1], JUN CHENG[1], MARK H. HORWITZ[1], and KELLY R. LEGAULT[2]

1. *School of Geosciences, University of South Florida, 4202 E. Fowler Ave., Tampa, FL 33620, USA. pwang@usf.edu*
2. *U.S. Army Corps of Engineers, Jacksonville District, 701 San Marco Blvd., Jacksonville, FL 32207 USA.*

Abstract: The dynamics of a dual inlet system in west-central Florida are investigated via field measurements and numerical modeling. This paper compares two commonly used numerical modeling systems, CMS and DELFT3D, in simulating the hydrodynamic and sediment transport processes. The model results are compared with various field data. Quantitatively as compared to point measurements, both models reproduced the measured nearshore wave accurately with a Willmott (1981) skill of 0.970 for CMS and 0.981for DELFT3D. Both models computed the flow through main inlet channel reasonably accurately although under-predicted the measured values. At the dominating John's Pass, the Willmott (1981) skill was 0.957 for CMS and 0.949 for DELFT3D. At the secondary Blind Pass, the Willmott skill was 0.989 for CMS and 0.938 for DELFT3D. Qualitatively, as compared to flow field measurements using a ship-mounted ADCP, both models captured key flow patterns including the ebb jet and alongshore flood flow. The models also yielded reasonable longshore current and interaction between longshore current and tidal flow. These flow patterns play significant roles in the morphodynamics of the ebb shoal and adjacent beaches.

Introduction

Simulating complex fields of wave, current, sediment transport, and morphology change in the vicinity of tidal inlets is a challenging task. When multiple inlets are involved, the case becomes even more complicated. Here we investigate the hydrodynamics and morphodynamics of John's Pass and Blind Pass inlets in west-central Florida based on field measurements and numerical modeling. The two inlets serve the same back-barrier bay and both are heavily structured. John's Pass is the dominant inlet of the two capturing 70-80% of the tidal prism.

Two commonly used numerical models, CMS and DELFT3D, were used to simulate the dynamics of the dual inlet system. CMS was developed by the Coastal Inlet Research Program at the US Army Corps of Engineers (Reed et al., 201l; Lin et al., 2011; Larson et al., 2011; Sanchez and Wu 2011) and has been used extensively in simulating inlet processes (Wang et al., 2011; Li et al., 2012). DELFT3D was developed by WL|Delft Hydraulics in cooperation with Delft University of Technology (Lesser et al. 2004) and has been applied to simulate coastal systems worldwide (Elias et al., 2012).

John's Pass and Blind Pass, separated by the 6-km long Treasure Island, service a portion of Boca Ciega Bay along the west-central Florida coast (Fig. 1). Regionally, the John's Pass-Blind Pass system is part of the west-central Florida barrier-island chain that extends north from the mouth of Tampa Bay. The entire area, from the beaches to the inlets to the back-bay, is densely developed since the 1930s. Several causeways and bridges and numerous dredge-and-fill finger channels dissect the back-barrier bay, especially within the water body landward of Blind Pass. The bay bathymetry is also artificially altered due to dredging and maintenance of the Intracoastal Waterway.

Fig. 1. Study area and field measurement locations and data collection time.

Study Area and Field Data Collection

The overall wave energy along this coast is mild with average breaker heights estimated to be 0.25-0.30 m (Wang and Beck, 2012). The study area is characteristic of a mixed tidal regime. The spring tide is typically diurnal with a range of roughly 0.8 to 1.2 m, whereas the neap tide is semi-diurnal with a range of 0.4 to 0.5 m. Sediments along the west-central Florida coast are bimodal composed of siliciclastic and carbonate fractions. The siliciclastic component is primarily fine quartz sand with a mean grain size of roughly 0.17 mm. The carbonate fraction is mostly shell debris of various sizes. Mean grain size in the study area varies typically from 0.17 mm to 1.00 mm, controlled by the varying amounts of shell debris. The largest grain sizes are found in the channel thalweg where coarse lag deposits are concentrated.

John's Pass is a jettied inlet located between Treasure Island to the south and Sand Key to the north. Since its opening in 1848 by a hurricane, John's Pass has gradually become the dominant inlet of the John's Pass-Blind Pass system

(Wang and Beck, 2012). The portion of Boca Ciega Bay landward of John's Pass is larger and not as dissected by man-made islands as compared to the portion landward of Blind Pass (Fig. 1). John's Pass has a large ebb shoal, skewed to the south due to the southward net longshore transport (Fig. 2). The channel-margin linear bar along the updrift (north) side, the relatively shallow terminal lobe, and the swash bar complex over the downdrift portion of the ebb shoal are illustrated by the detailed bathymetry. The downdrift attachment point where the bypassed sand reaches the beach is outlined by the protruding shoreline. Sunshine Beach updrift of the attachment point experiences chronic erosion, whereas the beach downdrift of the attachment point has up to 300 m of dry beach, and has shown an accretionary trend over the last two decades.

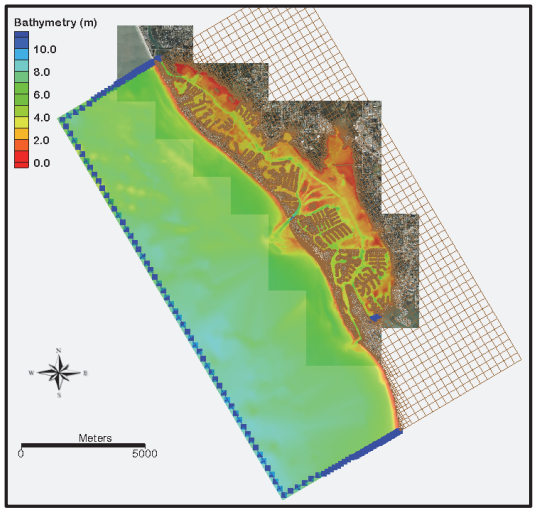

Fig. 2. CMS model domain of the John's Pass-Blind Pass system. DELFT3D domain is similar. Note the complicated bathymetry and development in the bay and southward skewed ebb shoals.

The origin of Blind Pass is not recorded. Prior to the opening of John's Pass in 1848, Blind Pass was the dominant inlet serving Boca Ciega Bay (Wang and Beck, 2012). As John's Pass gradually captured the majority of the tidal prism, the net longshore transport caused rapid southward migration of Blind Pass. It was eventually stabilized with jetties constructed since 1937, fixing the entrance channel into a 90-degree turn with a relatively wide (160 m) entrance channel, which became an effective trap for the southward longshore transport. Without an ebb shoal over several decades, little sand bypassed to the eroding downdrift beach. A small ebb shoal was developed since the last dredging in 2010 (Fig. 2).

As part of an inlet management study, a series of field measurements were conducted. One goal is to establish a verified numerical model of the dual inlet

system. Detailed bathymetry of the ebb shoals and channels, nearshore, and bay was captured with multi-beam and single beam surveys (Fig. 2). Water level and wave conditions were measured ~7 km offshore, providing boundary conditions for the numerical models. Several methods were used to measure the flow field. An upward-looking ADCP was deployed in the main channel of each inlet to measured current profiles. A side-looking ADCP was deployed at each inlet to measured cross-channel distribution of the flow. A ship-mount ADCP was used to map the flow field, particularly the ebb jet. Six synchronized tide gages were deployed in the bay to monitor water-level variations. A directional wave gage was deployed just seaward of the closure depth at about 300 m from the shoreline to measure nearshore wave conditions. Detailed analyses and interpretation of the field data are beyond the scope of this paper.

Here we use the field data to examine and compare two numerical models, CMS and DELFT3D, in simulating a dual inlet system. Nearly identical model domains (Fig. 2) were constructed. A 36-day record of water level and wave conditions measured at the seaward boundary (Fig. 1) were used to drive the numerical model (Fig. 3). Nearshore waves and currents measured at various locations were used to verify and compare the results from the two models. Wave-driven longshore current and its interaction with tidal current play a key role in inlet dynamics. A schematic model run simulating a northerly approaching energetic wave was conducted to examine the ability of the two models in simulating this process.

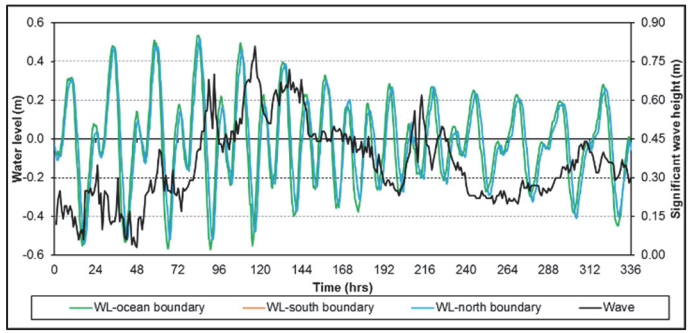

Fig. 3. Input water level and wave conditions for both CMS and DELFT3D.

Results

The CMS and DELFT3D models are driven by identical measured water level and wave boundary conditions for coupled wave-flow runs. Rectangle grids are used for both models. Due to different grid refining schemes and user interface support, the CMS and DELFT3D model grids are not identical. However, both models have similar spatial resolutions, e.g., at the inlet channels, back bay, and

nearshore area. In the following, the modeling results are compared with the measured data and with each other.

Modeled and measured wave conditions

Overall, both models propagated the waves accurately. Various friction factors were tested. The computed waves at the nearshore gage are not too sensitive to the friction coefficients for both models. Figure 4 illustrates the results using default friction coefficients. The wave heights were generally small over the 2-month study period. Several higher wave events were generated by cold front passages toward the end of the study period. CMS tends to over-predict the low waves, while DELFT3D tends to under-predict the high waves associated with the cold front passages. The Willmott (1981) skill (Eq. 1) is used to provide an overall comparison of the modeled and measured wave height.

$$S_w = 1 - \frac{\sum(V_{model} - V_{measure})^2}{\sum(|V_{model} - \overline{V_{measure}}| + |V_{model} - \overline{V_{model}}|)} \quad (1)$$

The Willmott skill is 0.970 for CMS and 0.981 for DELFT3D, indicating accurate prediction of wave height, with DELFT3D slightly better.

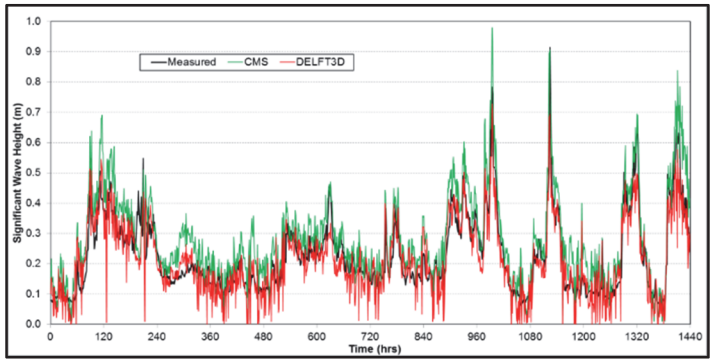

Fig. 4. Measured and modeled wave height just seaward of the closure depth (~4 m).

Modeled and measured currents

Flow velocities through the main channels at both inlets were measured using upward-looking ADCPs and compared with calculated values by the models. The manning's coefficient of 0.02, slightly smaller than the default value of 0.025, yielded the velocities that are closest to the measured values, and are shown here. Both models reproduced the measured velocities well, although both under-predicted the measured values (Fig. 5). CMS closely predicted the ebb velocity but under-predicted the flood velocity, while DELFT3D reproduced the flood velocity closer to the measured values but further under-predicted the

ebb velocity (Fig. 5). The Willmott skill of CMS and DELFT3D for predicting the John's Pass velocity is 0.957 and 0.949, respectively.

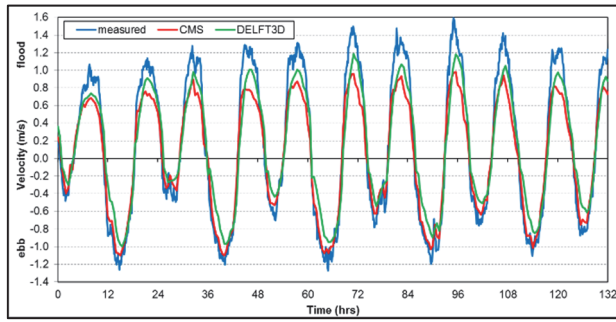

Fig. 5. Measured and modeled current velocity at John's Pass main channel.

Being the secondary inlet, both ebb and flood velocities through Blind Pass are smaller than those at John's Pass. Both models reproduced the measured flow well, although slightly lower than the measured values (Fig. 6). CMS performed very well with a Willmott skill of 0.989, higher than the 0.938 for DELFT3D.

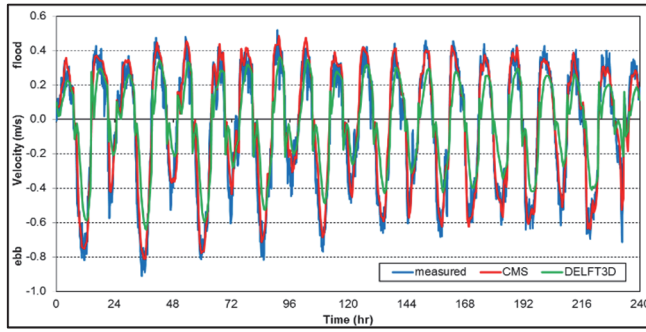

Fig. 6. Measured and modeled current velocity at Blind Pass main channel.

The under-prediction by the models at both inlets (Figs. 5 and 6) is likely related to the complicated bathymetry and land features in the bay. Sensitivity tests indicate that artificially increasing the bay water depth results in higher computed flow velocities. It is worth noting that both models allow spatially variable friction coefficients. Examining the influence of variable friction factors is beyond the scope of this paper.

Modeled flow patterns in the vicinity of the inlets

Tidal flow patterns in the vicinity of inlets, such as the ebb jet, alongshore flood flow, and interactions between tidal flow and wave-driven longshore current

play crucial roles in inlet dynamics and nearby beach processes. The models should capture key flow patterns and tide-wave interactions. In the following, modeled flow patterns are discussed and compared qualitatively with field data.

The overall flow patterns computed by the two modes are similar (Fig. 7). As expected, John's Pass services most of the bay, while Blind Pass tidal prism is limited to the south end of the domain. The relatively high velocity in the channel connecting to the large Boca Ciega Bay (bounded by a water-level boundary) to the east of the Blind Pass channel was not captured by DELFT3D. The tidal driven high velocity there was observed in the field.

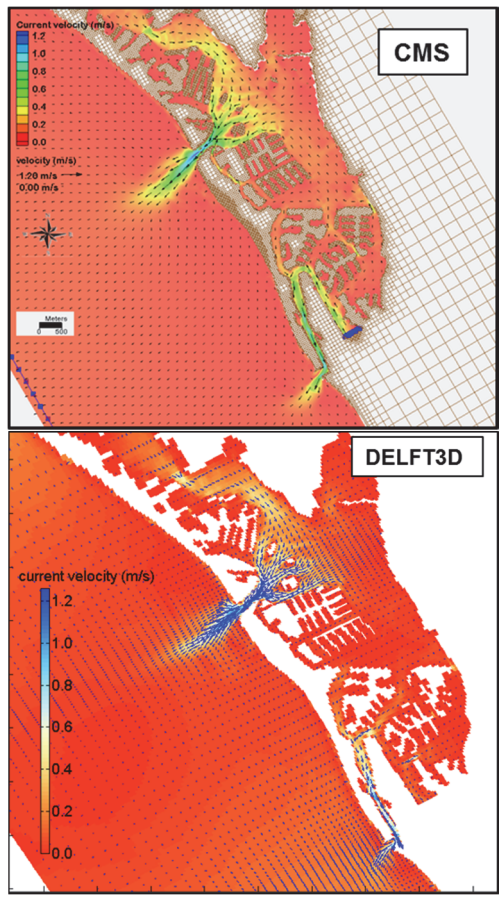

Fig. 7. Modeled flow field during a peak spring ebbing event at both John's Pass and Blind Pass.

Ebb jet plays an essential role in the formation of ebb shoals and in sand bypass around the inlet. The ebb jets at both John's Pass and Blind Pass were mapped

using a ship-mount ADCP. At John's Pass, the ebb jet extended seaward of the entrance to nearly 1.5 km (Fig. 8). The velocity decreases seaward as the jet spread wider. Both CMS and DELFT3D captured qualitatively the seaward and lateral extents and magnitude of the ebb jet. The slight southward skew of the ebb jet is also captured by the models. It is worth noting that the measured velocities are not simultaneous. Instead, they represent a portion of ebbing during a spring tide. The goal here is to compare the overall shape of the ebb jet.

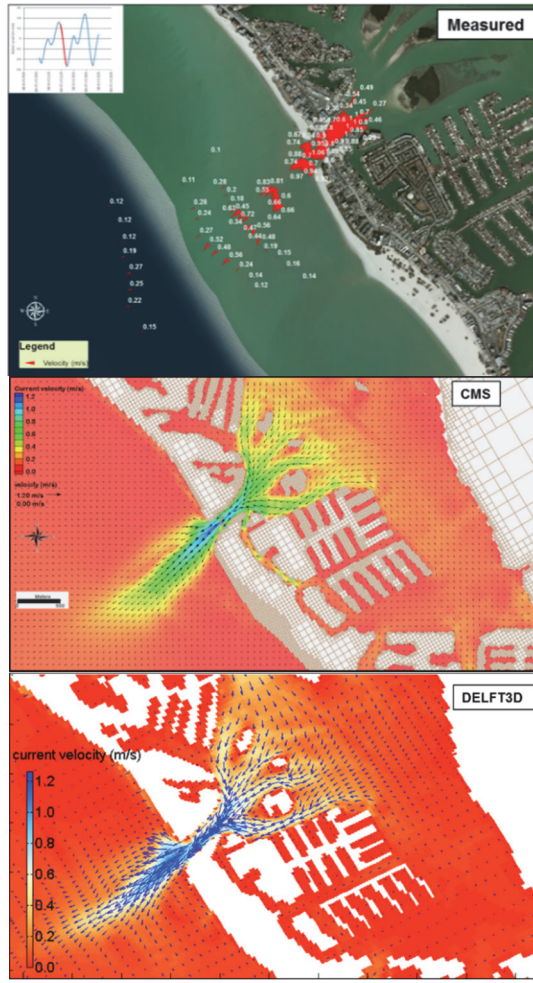

Fig. 8. Measured and modeled flow field during a peak spring ebbing event at both John's Pass.

The ebb jet at Blind Pass does not extend seaward as far as the John's Pass ebb jet (Fig. 9), likely due to the weaker flow and the 90-degree turn of the main

channel. The flow patterns at the bent, e.g., weaker flow at the corner and strong flow along the south side, are captured by the models and are comparable to the measured pattern. This flow pattern is crucial to the sediment deposition pattern at the 90-degree inlet (Wang and Beck, 2012).

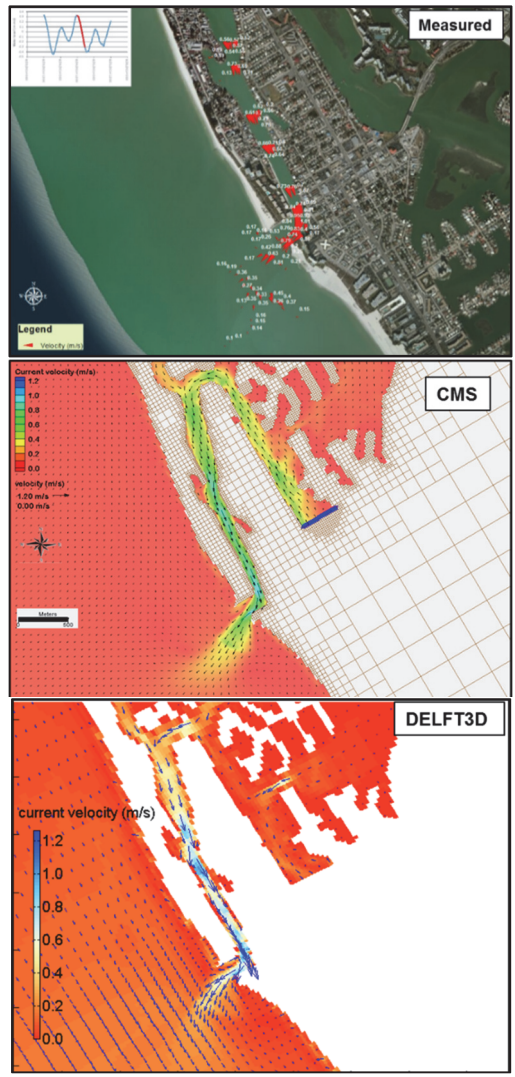

Fig. 9. Measured and modeled flow field during a peak spring ebbing event at both John's Pass.

Flood tide current does not extend farther seaward. Instead, a longshore current is modeled along the immediate adjacent beaches. This longshore flow, often

observed during field surveys, has significant implications on adjacent beach processes. Specifically, it contributes to the chronic erosion at Sunshine Beach directly south of John's Pass. Both CMS and DELFT3D captured the flood current pattern well as compared qualitatively to the measured pattern (Fig. 10).

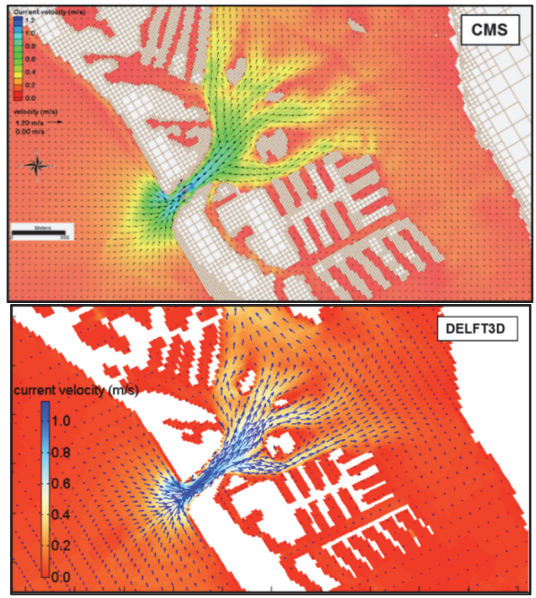

Fig. 10. Modeled flow field during a peak spring flooding event at John's Pass.

At Blind Pass, due to the 90-degree turn, flood flow (Fig. 11) follows a different pattern as that of ebb current (Fig. 9). Ebb flow focuses along the south side while flood flow distribute uniformly across the entrance channel. This results in a relatively stronger ebb flow along the south side, corresponding to the deep channel there. Along the north side, sediment input from the southward longshore transport combined with weak ebb flushing leads to sedimentation. Both models captured this difference between ebb and flood, which is essential to modeling the scour and sedimentation in the 90-degree channel.

Longshore current and its interaction with tidal flow play a significant role in the morphodynamics of the ebb shoal and nearby beaches. For the studied coast, winter cold front passages contribute significantly to the generation of energetic conditions and the southward net longshore transport (Wang and Beck, 2012). A schematic model run was conducted simulating an energetic northerly incident wave, with a significant wave height of 1.5 m, peak period of 5.7 s, and incident angle of 300 degrees, during a spring-neap tidal cycle. Both DELFT3D and CMS yielded longshore current velocities of 0.2 to 0.4 m/s (Fig. 12).

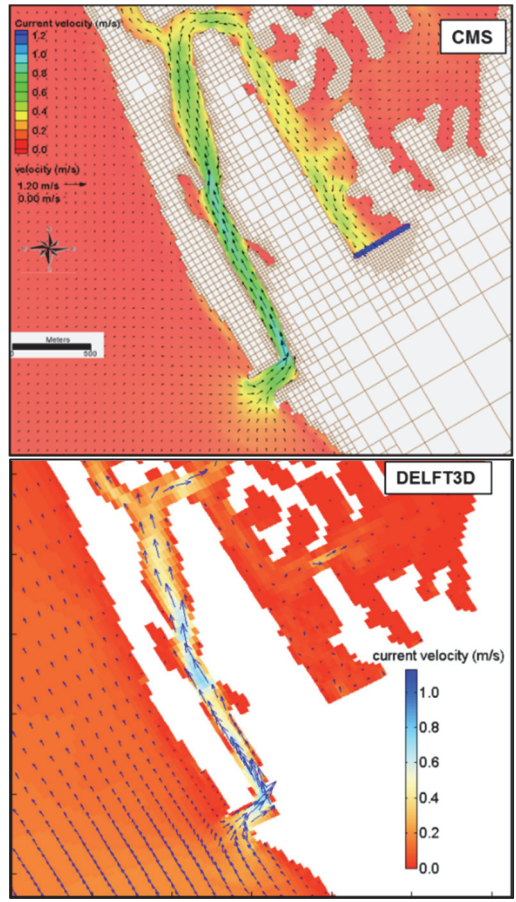

Fig. 11. Modeled flow field during a peak spring flooding event at Blind Pass.

The interaction of the longshore current with ebb jet at John's Pass includes converged flow directed offshore on the updrift side and a gyre on the downdrift side. The converging longshore current and ebb jet provides the processes for the development of ebb shoal and channel margin linear bar. The gyre and the diverging flow explain the chronic erosion along the beach there. Both CMS and DELFT3D captured key dynamic processes of inlet-beach interaction.

At Blind Pass, both models predict that the longshore current flows into the inlet, merges with ebbing flow and exits the inlet along the south side (Fig. 13). This process is responsible for the deposition along the updrift side of the inlet (Wang et al., 2007). Downdrift of the inlet, the longshore current resumes along the chronic eroding Upham Beach. Therefore, both models correctly reproduced the process that is responsible for the beach erosion there.

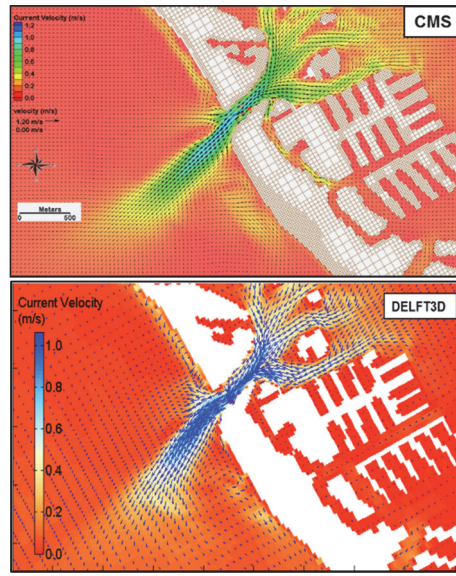

Fig. 12. Interaction of a southward longshore current and ebb jet at John's Pass.

Summary and Conclusions

Extensive field data were collected at John's Pass-Blind Pass dual inlet system, including 1) detailed bathymetry; 2) offshore and nearshore wave conditions; 3) current profiles in the main channels; 3) flow velocity distributions across the main channels; 4) flow field in the vicinity of the inlet; and 5) water-level fluctuations at six locations in the back bay. This field dataset was used here to examine two numerical model systems, CMS and DELFT3D. Similar modeling domains were constructed based on bathymetry data collected by this study. The coupled wave-current model runs are driven by identical measured boundary conditions. The model results are compared with field data and with each other. The models, specifically the friction coefficient, were calibrated and verified with the field data. The same friction coefficient was used for both models to ensure compatibility of the results. Implicit versions of both models were used in this study. A 36-day simulation was conducted and compared here. The speed of the coupled wave and current model runs was similar for the two models.

The modeled waves compared well with the measured nearshore conditions. For wave height, the Willmott (1981) skill was 0.970 for CMS and 0.981 for DELFT3D, both indicating accurate modeling. The computed flood and ebb velocities through the main channels are lower than the measured values. At John's Pass, the Willmott skill was 0.957 for CMS and 0.949 for DELFT3D. At Blind Pass, the Willmott skill was 0.989 for CMS and 0.938 for DELFT3D.

The model results are compared qualitatively with the flow field measurement using a ship-mount ADCP. Both models captured key flow patterns including the ebb jet and alongshore flood flow. The models also yielded reasonable longshore current velocity and interaction of longshore current and tidal flow. These spatial flow patterns play significant roles in inlet morphodynamics such as formation of ebb shoal, sand bypass around the inlet, erosion and accretion at adjacent beaches. Future study will include longer-term run, e.g., for 1-2 years, to compare with measured morphology changes.

Acknowledgements

This study is partially funded by the University of South Florida and US Army Corps of Engineers Coastal Inlet Research Program. Field data collection is supported by numerous graduate students.

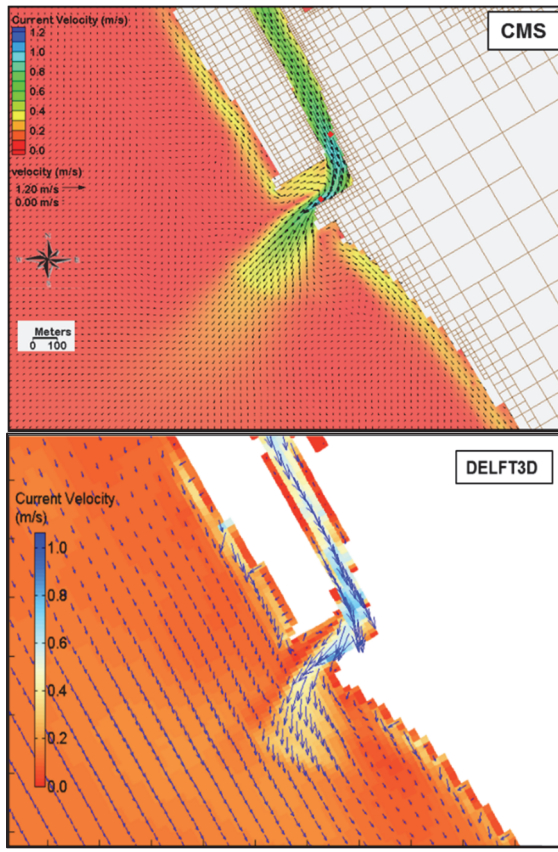

Fig. 13. Interaction of a southward longshore current and ebb jet at Blind Pass.

References

Elias, E. P. L., Gelfenbaum, G., and Van der Westhuysen, A.J. (2012). "Validation of a coupled wave-flow model in a high-energy setting: The mouth of the Columbia River," *Journal of Geophysical Research*, 117, C09011, doi:10.1029/2012JC008105.

Larson M., Camenen B., and Pham T.N. (2011). "A unified sediment transport model for inlet application," *Journal of Coastal Research*, Special Issue 59, 27-38.

Lesser G.R., Roelvink, J.A., van Kester, J.A.T.M., and Stelling G.S. (2004). "Development and validation of a three-dimensional morphological model," *Coastal Engineering*, 51, 883-915.

Li, H.; Lin, L., and Burks-Copes, K.A. (2013). "Modeling of coastal inundation, storm surge, and relative sea-level rise at Naval Station Norfolk, Norfolk, Virginia, U.S.A," *Journal of Coastal Research*, 29(1), 18-30.

Lin L., Demirbileb Z., and Mase H. (2011). "Recent capabilities of CMS-Wave: a coastal wave model for inlets and navigation projects;" *Journal of Coastal Research*, Special Issue 59, 7-14.

Reed C.W., Brown M.E., Sanchez A., Wu W., and Buttolph, A.M. (2011). "The coastal modeling system flow model (CMS-FLOW): past and present," *Journal of Coastal Research*, Special Issue 59, 1-6.

Sanchez A., and Wu W. (2011). "A non-equilibrium sediment transport model or coastal inlet and navigational channel," *Journal of Coastal Research*, Special Issue 59, 39-48.

Wang, P., Beck T.M., and Roberts T.M. (2011). "Modeling regional-scale sediment transport and medium-term morphology change at a dual inlet system examined with the Coastal Modeling System (CMS): A case study at Johns Pass and Blind Pass, west-central Florida," *Journal of Coastal Research*, Special Issue 59, 49-60.

Wang P., and Beck T.M. (2012). "Morphodynamics of an anthropogenically altered dual-inlet system: John's Pass and Blind Pass, west-central Florida, USA," *Marine Geology*, 291-294, 162-175.

Wang,P., Tidwell, D.K., Beck, T.M., and Kraus, N.C. (2007). "Sedimentation patterns in a stabilized migratory inlet, Blind Pass, Florida," *Proceedings of Coastal Sediments07*, ASCE Press, 1377-1390.

Willmott, C. J. (1981). "On the validation of models," *Physical Geography*, 2, 184-194.